Optical imaging of objects in turbid media using heterodyned optical Kerr gate

Pingping Zhan, Wenjiang Tan, Jinhai Si, Shichao Xu, Junyi Tong, and Xun Hou

Citation: Applied Physics Letters **104**, 211907 (2014); doi: 10.1063/1.4880115
View online: http://dx.doi.org/10.1063/1.4880115
View Table of Contents: http://scitation.aip.org/content/aip/journal/apl/104/21?ver=pdfcov
Published by the AIP Publishing

Optical imaging of objects in turbid media using heterodyned optical Kerr gate

Pingping Zhan (占平平),[1] Wenjiang Tan (谭文疆),[1,a)] Jinhai Si (司金海),[1] Shichao Xu (许士超),[1] Junyi Tong (佟俊仪),[2] and Xun Hou (侯洵)[1]
[1]*Key Laboratory for Physical Electronics and Devices of the Ministry of Education and Shaanxi Key Laboratory of Information Photonic Technique, School of Electronics and Information Engineering, Xi'an Jiaotong University, Xianing-xilu 28, Xi'an 710049, China*
[2]*Departments of Applied Physics, Xi'an University of Technology, Xi'an 710048, China*

(Received 26 January 2014; accepted 15 May 2014; published online 29 May 2014)

In this paper, we demonstrated optical imaging of objects hidden behind highly turbid media with a femtosecond heterodyned optical Kerr gate (HOKG). The experimental results showed that when compared with traditional optical Kerr gated (OKG) imaging, the HOKG imaging system provided higher image sharpness and higher spatial resolution. In traditional OKG imaging system, low pass filtering due to a photoinduced soft aperture decreased the image sharpness. When the HOKG was used, the high spatial frequency components of the object could be effectively compensated. © *2014 AIP Publishing LLC*. [http://dx.doi.org/10.1063/1.4880115]

Light propagating through a random medium undergoes multiple scattering. Multiple scattering of photons affects the fidelity of optical information that is carried by the transiting photons. This situation can occur in many cases, such as inferior visibility through fogs and imaging of embedded objects in turbid media. In a random medium, owing to multiple light scattering, the incident light is split into three components, ballistic photons, quasi-ballistic photons, and scattered photons.[1] The ballistic photons propagate through the medium undeviated in the forward direction and carry the information about objects behind or inside the medium. The quasi-ballistic photons, also called as snake photons, travel close to their initial trajectory and also carry useful information about the internal objects along their propagation.[2,3] The scattered photons undergo random scattering in all directions and provide no useful information. In order to see an object hidden in or behind a highly scattering random medium, useful information must be selected carefully from such scattered light for imaging through turbid media. For objects in turbid media, optical imaging methods are critical tools in fields such as medical diagnosis,[4] fluid dynamics measurements,[5] detection of combustion of a high-speed rocket spray,[6–8] and materials science.[9]

The image quality of an object in turbid media can be enhanced by using the time-gated imaging technique.[10,11] This technique makes using of a very fast shutter to select the ballistic and quasi-ballistic photons from the imaging pulse. Most of the time-gated imaging systems depend on the optical Kerr gate (OKG) technique.[12–17] The optical Kerr gate is based on the optical Kerr effect, and the shutter time can be up to tens of femtoseconds. To improve the image contrast and signal-to-noise ratio of hidden objects in turbid media, most of the OKG imaging systems typically use the "Kerr-Fourier" imaging configuration.[18] However, the gating beam induces a transient aperture in the Kerr material in the imaging system, which filters some high spatial frequency components of the detected object. Therefore, the sharpness of the images and spatial resolution of the imaging system decreases. Although locating the optical Kerr medium in an image plane can eliminate the effects of low-pass filtering, this will result in considerably noisy images because of scattering of the light from the gating pulse.

In this study, we proposed a femtosecond heterodyned optical Kerr gate (HOKG) imaging technique for imaging objects hidden behind turbid media. The HOKG can compensate the high spatial frequency components of the objects, which are filtered by a photoinduced soft aperture in traditional OKG imaging. The experimental results show that when compared with traditional OKG imaging, HOKG imaging enhances image sharpness and provides a higher spatial resolution of the imaging system.

The schematic of the ballistic imaging system used in our experiments is shown in Fig. 1(a). A Ti:sapphire laser system (Coherent Inc., Libra-USP-HE) having a repetition rate of 1 kHz and a pulse duration of 50 fs at 800 nm was used in our experiments. The output beam was split into two beams with a short-pass filter (SPF: Newport Corporation, 10SWF-800-B), and two neutral attenuators (NA1 and NA2) were used to adjust their intensities. The reflective part was used as the imaging beam, and the transmitted part was used as the gating beam. The imaging beam was modulated by a 1.41 line pair (lp)/mm section of the resolution test target (a United States Air Force resolution target) and then introduced into the turbid media. Thereafter, this imaging beam transmitted through the turbid media was collected by a lens (L1) and focused onto an ultrafast OKG.

As shown in Fig. 1(b), in traditional OKG, the polarization direction of the polarizer is horizontal, and the polarization direction of the analyzer is vertical, but the polarization direction of the analyzer is rotated at an angle of θ from the vertical direction in HOKG. In Fig. 1(b), the black circle spots on the optical Kerr material represent the spatial Fourier spectrum of the object. Here, the low spatial frequency components were located at the center of the spatial Fourier spectrum, which determines the profile of the object. The high frequency components were located away from the center of

a)Electronic mail: tanwenjiang@mail.xjtu.edu.cn

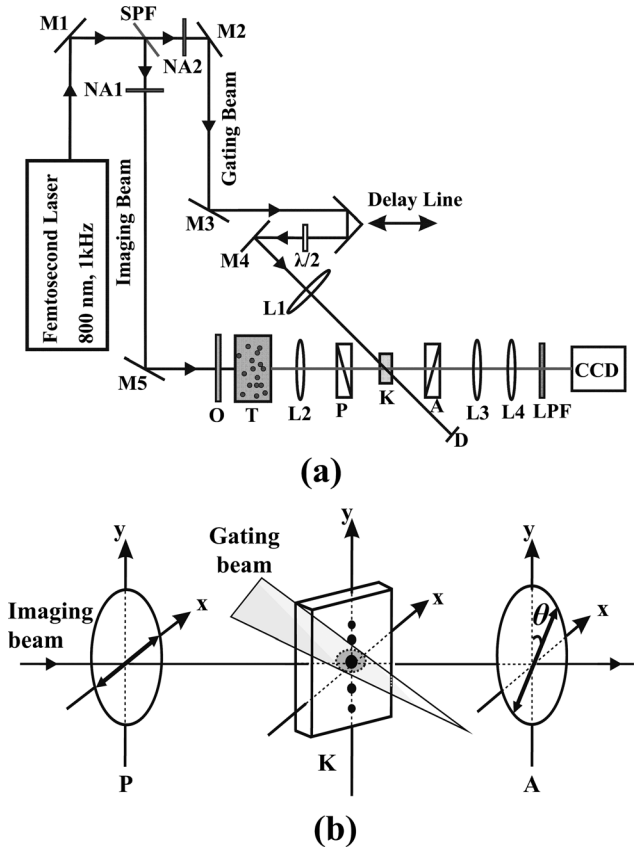

FIG. 1. (a) Schematic of the ballistic imaging system. (b) Schematic of HOKG in which the black circle spots and the gray circle region on the optical Kerr material represent the spatial frequency components of the object and the nonlinear interaction region of the gating and imaging beams, respectively. (Note that SPF: short-pass filter; NA1, NA2: neutral attenuators; $\lambda/2$: half-wave plate; O: object; T: turbid media; P: polarizer; K: optical Kerr material; A: analyzer; OKG: optical Kerr gate; D: dump; LPF: long-pass filter; M1, M2, M3, and M4: mirrors; L1, L2, L3, and L4: lenses.)

the spatial Fourier spectrum, which determines small structures and fine details of the object. The nonlinear interaction region of the gating and imaging beams was also indicated by a gray circle region in Fig. 1(b). In addition, 0.5-cm-thick polystyrene microsphere suspensions having a diameter of 3.13 μm were used as the turbid media. The Kerr medium was a 1 mm Te glass. The gating beam, passing through an optical delay translation and a half-wave plate ($\lambda/2$), was focused onto an optical Kerr material by a lens (L2). The half-wave plate was used to control its polarization for maximum gating efficiency. When the OKG was opened by the gating pulse, part of the imaging beam passed through the analyzer. By adjusting the time delay between the gating pulse and imaging pulse, the ballistic component of the imaging beam could be temporally selected by the OKG. The OKG imaging beam was subsequently collected by two lenses (L3, L4) and imaged onto a CCD camera (Lumenera INFINITY 3-1). A long-pass filter (LPF: Newport Corporation, 10LWF-800-B) was placed between L4 and the camera to decrease the intensity of noise generated by the pump pulse scattering in the optical Kerr medium. It should be noted that the background noise for the HOKG imaging was considerable when the analyzer was rotated at a heterodyned angle. Therefore, the background noise of the HOKG image was measured by blocking the gating pulse and subtracted.

An essential aspect of an optical system is its ability to transmit spatial information and the relevant parameter for evaluating performance is image visibility. We first measured three typical images of an object hidden behind highly turbid media with direct (without OKG), OKG, and HOKG imaging as shown on the left side of Fig. 2. Here, an USAF resolution target was used as the detected object and 0.5-cm-thick suspensions of 3.13 μm polystyrene microspheres at OD = 9.3 were used as the turbid media. OD is the optical density. The heterodyned angle was $-3°$. From the left side of Figs. 2(a)–2(c), we can see that the image visibility of direct imaging is worse than that of OKG and HOKG imaging in which the scattering photons were imaged as noise. When compared with direct imaging, a better image can be obtained with OKG and HOKG imaging due to removal of the scattering photons.

To further compare the image sharpness for direct, OKG, and HOKG imaging, the enlarged two-dimensional spatial intensity distributions in the white rectangular areas are also shown in Fig. 2. In the direct imaging case, the shadowed and unshadowed regions cannot be identified clearly, as shown on the right side of Fig. 2(a). In the OKG imaging case, the shadowed and unshadowed regions of the image can be identified more clearly as shown on the right side of Fig. 2(b). However, the boundaries of the shadowed and unshadowed regions are slightly blurred. This could be attributed to the transient soft aperture induced by the gating beam in the Kerr material, which filtered some high spatial frequency components of the object.

When HOKG is used, the boundaries of the image can be more clearly identified as shown on the right side of Fig. 2(c) in which the high spatial frequency components of the imaged objects were partly compensated. It can be explained as follows. For a HOKG as used in our experiment, the gated light intensity can be written in the following form:[19]

$$I_{\text{signal}} \propto H^2{}_{\text{real}} + H^2{}_{\text{imaginary}} - 2\theta E_{\text{probe}} H_{\text{imaginary}}. \quad (1)$$

When a quarter-wave plate is placed in front of the analyzer, with its optical axis parallel to the polarization direction of the probe beam, the HOKG signal is then given by[19]

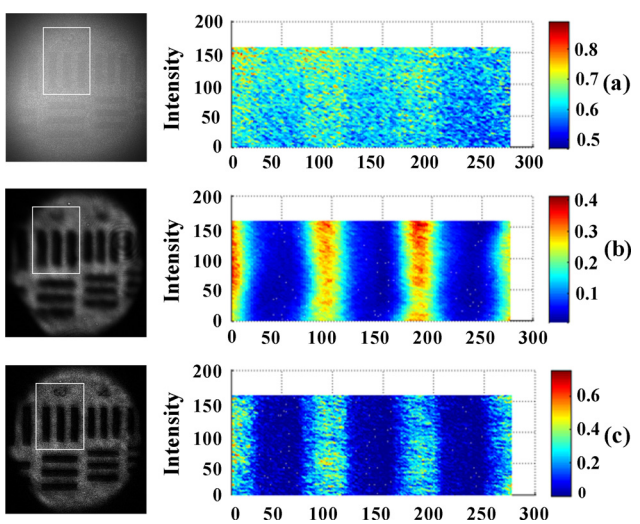

FIG. 2. Comparison of image visibilities and two-dimensional spatial intensity distributions of images obtained at OD = 9.3 using (a) direct, (b) OKG, and (c) HOKG imaging.

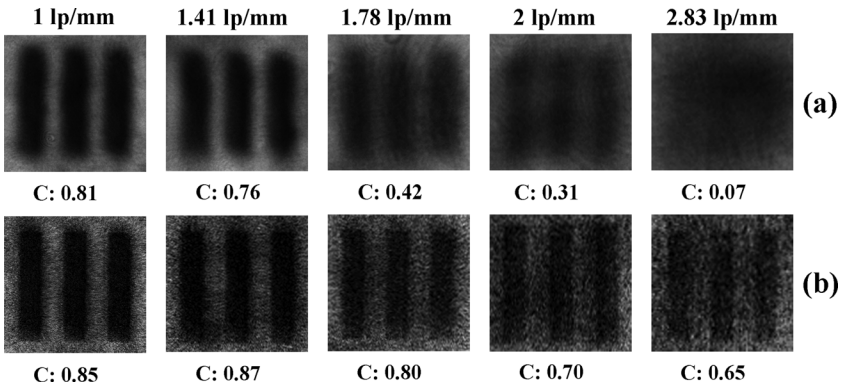

FIG. 3. Comparison of image visibilities and the corresponding image contrasts using (a) OKG and (b) HOKG imaging. (C: contrast.)

$$I_{\text{signal}} \propto H^2{}_{\text{real}} + H^2{}_{\text{imaginary}} - 2\theta E_{\text{probe}} H_{\text{real}}. \quad (2)$$

Here, the term $H^2{}_{\text{real}} + H^2{}_{\text{imaginary}}$ is the normal optical Kerr signal term. The field amplitudes H_{real} and $H_{\text{imaginary}}$ represent the real and imaginary parts of nonlinear response, respectively. The terms $2\theta E_{\text{probe}} H_{\text{imaginary}}$ or $2\theta E_{\text{probe}} H_{\text{imaginary}}$ are the heterodyne signal terms. θ is the heterodyne angle, and E_{probe} represents the optical electric field of the probe beam. The H_{real} arises from photon-induced birefringence. Usually, the $H_{\text{imaginary}}$ arises from several possible physical mechanisms, such as photon-induced dichroism, transient grating, and nonlinear absorption. In our experiment, the $H_{\text{imaginary}}$ can be mainly attributed to the photon-induced dichroism, because the photo-induced transient grating has been eliminated by using a short-pass filter to split the output laser into the imaging and the gating beams.[20] In addition, the possibility of the nonlinear absorption has also been excluded with the help of a nonlinear transmittance measurement.[21] For the OKG imaging, the normal optical Kerr signal ($H^2{}_{\text{real}} + H^2{}_{\text{imaginary}}$) only contains the low spatial frequency components of the object due to the photo-induced transient soft aperture effect. For the HOKG imaging, the heterodyne signals ($2\theta E_{\text{probe}} H_{\text{imaginary}}$ or $2\theta E_{\text{probe}} H_{\text{real}}$) contain more high spatial frequency components of the object comparing with normal optical Kerr signal because the heterodyne signal is proportional to the product of the local oscillator ($\sim\theta E_{\text{probe}}$) and the nonlinear response fields ($H_{\text{imaginary}}$ or H_{real}) and the E_{probe} contains almost all spatial frequency components of the object because it is not involved in the nonlinear optical Kerr effect. Therefore, the HOKG imaging can partially compensate the high spatial frequency components of the object in which the heterodyne signal provides a signal gain.

It should be mentioned that although the image sharpness for the HOKG imaging is improved obviously comparing with the OKG image as shown in Fig. 2, the HOKG image intensity only increased by about 2%. This is because the nonlinear response field $H_{\text{imaginary}}$ was weak for the transparent optical Kerr material used in our experiment. To further enhance the heterodyne signal intensity, a feasible way is to make use of the photo-induced birefringence H_{real} by placing a quarter-wave plate in front of the analyzer as shown in Eq. (2) because H_{real} is much larger than $H_{\text{imaginary}}$ for transparent optical Kerr materials.

Furthermore, we compared the image contrasts for OKG and HOKG imaging. Figure 3 shows serials of images of the resolution test patterns and the corresponding image contrasts. The spatial frequencies of the resolution test patterns were 1, 1.41, 1.78, 2, and 2.83 lp/mm, the bar widths of which were 500, 354, 281, and 177 μm, respectively. From Fig. 3(a), we can see that the image contrasts for OKG imaging decreased from 0.81 to 0.07 with varying the spatial frequency of the object from 500 μm to 177 μm in our experiment. Here, the contrast was calculated by the following formula $Contrast = (I_{\max} - I_{\min})/(I_{\max} + I_{\min})$, where $I_{\max}$ is the average light intensity corresponding to the unshadowed region of the imaged resolution test pattern and $I_{\min}$ is the average light intensity corresponding to the shadowed region. This is because the Fourier spectral profile of an object would increase with increasing its spatial frequency.[22] Thus, for OKG imaging, the image contrasts decreased more seriously with decreasing the object size due to losing more higher spatial frequency components. From Fig. 3(b), we can see that the image contrasts for HOKG imaging decreased slightly from 0.85 to 0.65 with increasing the spatial frequency of the object. Comparing with OKG imaging, a better image contrast can be obtained for HOKG imaging due to compensating some high frequency components of the object.

As described above, HOKG imaging can partly compensate the high spatial frequency components of the object. However, some scattering photons in the local oscillator ($\sim\theta E_{\text{probe}}$) for HOKG imaging are also introduced into the CCD camera as the background noise. Figure 4 shows the dependence of normalized heterodyned optical Kerr gated signal-local oscillator signal (HOKGS-LOS) ratio on the

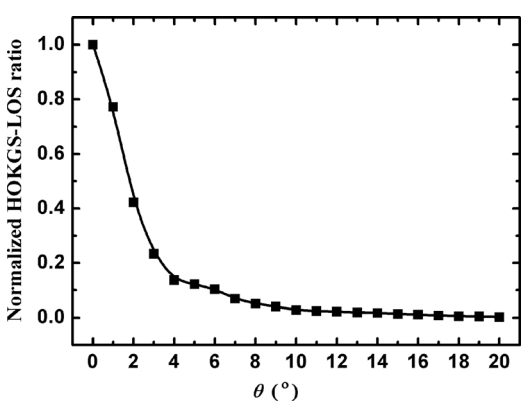

FIG. 4. Dependence of normalized HOKGS-LOS ratio on the heterodyne angle θ.

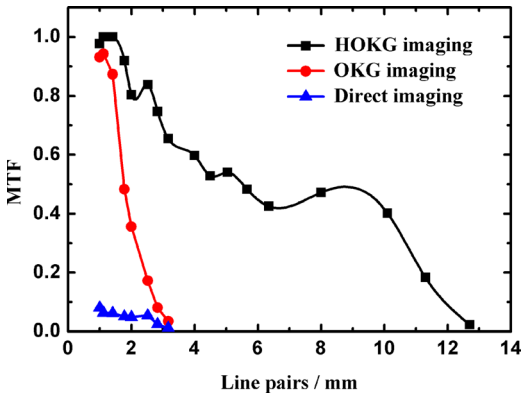

FIG. 5. Comparison of the MTF of the direct, OKG, and HOKG imaging systems.

heterodyne angle. Here, the local oscillator signal was measured by blocking the gating pulses. From Fig. 4, we can see that the HOKGS-LOS ratio decreases with increasing the heterodyne angle θ. So, for HOKG imaging, an optimal heterodyne angle θ should be chosen to avoid introducing too much background noise, meanwhile, to ensure enough heterodyne signal intensity. It should be indicated that a small background noise could be easy measured by blocking the gating pulse and subtracted in the image processing.

Finally, to evaluate the performance of the direct, OKG, and HOKG imaging system, we measured the modulation transfer function (MTF) for these three imaging systems. The MTF was given as $\mathrm{MTF} = C_i/C_{ref}$, where C_i represents the contrast for a resolution test pattern measured and the reference contrast C_{ref} was determined by the contrast of the resolution test pattern with lowest spatial frequency in the image. In our experiment, C_{ref} equals to C (1 lp/mm). From Fig. 5, we can see that the spatial resolution is higher with HOKG imaging than with direct and OKG imaging. The maximum resolvable spatial frequency is 13 lp/mm, and the corresponding resolved object size is approximately 40 μm in our experiments. However, the maximum resolvable spatial frequency is the same (3.17 lp/mm) for direct and OKG imaging, which corresponds to a resolved object size of approximately 157 μm. The results show that the HOKG could compensate the high spatial frequency components of the object, thus increasing the sharpness of boundaries and providing a higher resolvable spatial frequency.

It should be noted that for OKG imaging, the image contrast and spatial resolution are dependent on the size and power of the pump beam. For example, the influence of low-pass filtering on OKG imaging could be weakened by increasing the diameter of the pump beam. However, increasing the diameter of the pump beam will decrease the power density of the gating beam, which can deteriorate the imaging visibility due to lower OKG transmittance at lower power densities. In addition, the transmittance of OKG can be increased by increasing the pump power. However, our previous research showed that when the pump power was increased to a certain extent, the profile of the gating beam might change from a Gaussian distribution to an annulus distribution,[23] which would tremendously disturb the image fidelity. Therefore, the pump power for HOKG imaging should be optimized to avoid the distortion of the imaging beam.

In summary, we investigated the ballistic imaging of objects hidden behind turbid media using a HOKG. The results show that for OKG imaging, the high frequency components were filtered by the photoinduced transient aperture in the Kerr medium. For HOKG imaging, the high spatial frequency components of the objects could be compensated, and images with higher image sharpness and spatial resolution can be obtained when compared with traditional OKG imaging.

The authors gratefully acknowledge the financial support for this work provided by the National Natural Science Foundation of China under the Grant Nos. 61235003, 61308036, and 61205129, the Fundamental Research Funds for the Central Universities (Grant No. xjj2012020), and the China Postdoctoral Science Foundation funded Project (No. 2013M540753).

[1]L. Wang, P. P. Ho, C. Liu, G. Zhang, and R. R. Alfano, Science **253**, 769 (1991).
[2]C. Dunsby and P. M. W. French, J. Phys. D: Appl. Phys. **36**, R207 (2003).
[3]Q. Z. Wang, X. Liang, L. Wang, P. P. Ho, and R. R. Alfano, Opt. Lett. **20**, 1498 (1995).
[4]P. P. Ho, P. A. Galland, X. Liang, L. Wang, S. G. Demos, S. K. Gayen, and R. R. Alfano, Proc. SPIE **2979**, 94 (1997).
[5]M. Linne, M. Paciaroni, T. Hall, and T. Parker, Exp. Fluids **40**, 836 (2006).
[6]D. Sedarsky, M. Paciaroni, E. Berrocal, P. Petterson, J. Zelina, J. Gord, and M. Linne, Exp. Fluids **49**, 391 (2010).
[7]D. Sedarsky, J. Gord, C. Carter, T. R. Meyer, and M. A. Linne, Opt. Lett. **34**, 2748 (2009).
[8]J. B. Schmidt, Z. D. Schaefer, T. R. Meyer, S. Roy, S. A. Danczyk, and J. R. Gord, Appl. Opt. **48**, B137 (2009).
[9]N. Fang, H. Lee, C. Sun, and X. Zhang, Science **308**, 534 (2005).
[10]M. Paciaroni and M. Linne, Appl. Opt. **43**, 5100 (2004).
[11]M. E. Zevallos, S. K. Gayen, M. Alrubaiee, and R. R. Alfano, Appl. Phys. Lett. **86**, 011115 (2005).
[12]T. Yasui, K. Minoshima, E. Abraham, and H. Matsumoto, Appl. Opt. **41**, 5191 (2002).
[13]M. Linne, M. Paciaroni, E. Berrocal, and D. Sedarsky, Proc. Combust. Inst. **32**, 2147 (2009).
[14]W. Tan, Y. Yang, J. Si, J. Tong, W. Yi, F. Chen, and X. Hou, J. Appl. Phys. **107**, 043104 (2010).
[15]J. Tong, Y. Yang, J. Si, W. Tan, F. Chen, W. Yi, and X. Hou, Opt. Eng. **50**, 043607 (2011).
[16]F.-X. d'Abzac, M. Kervella, L. Hespel, and T. Dartigalongue, Opt. Express **20**, 9604 (2012).
[17]W. Tan, Z. Zhou, A. Lin, J. Si, P. Zhan, B. Wu, and X. Hou, Opt. Express **21**, 7740 (2013).
[18]L. Wang, P. P. Ho, X. Liang, H. Dai, and R. R. Alfano, Opt. Lett. **18**, 241 (1993).
[19]M. E. Orczyk, M. Samoc, J. Swiatkiewicz, and P. N. Prasad, J. Chem. Phys. **98**, 2524 (1993).
[20]J. Tong, W. Tan, J. Si, Y. Yang, W. Yi, F. Chen, and X. Hou, J. Appl. Phys. **109**, 123104 (2011).
[21]T. Boggess, K. Bohnert, K. Mansour, S. C. Moss, I. Boyd, and A. Smirl, IEEE J. Quantum Electron. **22**, 360 (1986).
[22]L. Wang, P. P. Ho, and R. R. Alfano, Appl. Opt. **32**, 5043 (1993).
[23]X. Wang, P. He, L. Yan, J. Si, F. Chen, and X. Hou, Appl. Phys. B **112**, 279 (2013).